



## Tropospheric Emission Spectrometer observations of the tropospheric HDO/H<sub>2</sub>O ratio: Estimation approach and characterization

John Worden,<sup>1</sup> Kevin Bowman,<sup>1</sup> David Noone,<sup>2</sup> Reinhard Beer,<sup>1</sup> Shepard Clough,<sup>3</sup> Annmarie Eldering,<sup>1</sup> Brendan Fisher,<sup>1</sup> Aaron Goldman,<sup>4</sup> Michael Gunson,<sup>1</sup> Robert Herman,<sup>1</sup> Susan S. Kulawik,<sup>1</sup> Michael Lampel,<sup>5</sup> Ming Luo,<sup>1</sup> Gregory Osterman,<sup>1</sup> Curtis Rinsland,<sup>6</sup> Clive Rodgers,<sup>7</sup> Stanley Sander,<sup>1</sup> Mark Shephard,<sup>3</sup> and Helen Worden<sup>1</sup>

Received 6 September 2005; revised 15 February 2006; accepted 13 April 2006; published 25 August 2006.

[1] We present global, vertical profile estimates of the HDO/H<sub>2</sub>O ratio from the Tropospheric Emission Spectrometer (TES) on the Earth Observing System (EOS) Aura satellite. We emphasize in this paper the estimation approach and error characterization, which are critical to determining the very small absolute concentration of HDO relative to H<sub>2</sub>O and its uncertainty. These estimates were made from TES nadir-viewing (downlooking) thermal infrared spectral radiances observed on 20 September 2004. Profiles of HDO and H<sub>2</sub>O are simultaneously estimated from the observed radiances and a profile of the ratio is then calculated. This simultaneous, or “joint,” estimate is regularized with an a priori covariance matrix that includes expected correlations between HDO and H<sub>2</sub>O. This approach minimizes errors in the profile of the HDO/H<sub>2</sub>O ratio that are due to overlapping HDO and H<sub>2</sub>O spectroscopic lines. Under clear-sky conditions in the tropics, TES estimates of the HDO/H<sub>2</sub>O ratio are sensitive to the distribution of the actual ratio between the surface and about 300 hPa with peak sensitivity at 700 hPa. The sensitivity decreases with latitude through its dependence on temperature and water amount. We estimate a precision of approximately 1% to 2% for the ratio of the HDO/H<sub>2</sub>O tropospheric densities; however, there is possibly a bias of approximately 5% in the ratio due to the HDO spectroscopic line strengths. These global observations clearly show increased isotopic depletion of water vapor at higher latitudes as well as increased depletion in the upper troposphere versus the lower troposphere.

**Citation:** Worden, J., et al. (2006), Tropospheric Emission Spectrometer observations of the tropospheric HDO/H<sub>2</sub>O ratio: Estimation approach and characterization, *J. Geophys. Res.*, *111*, D16309, doi:10.1029/2005JD006606.

### 1. Introduction

[2] The isotopic distribution of water vapor has increasingly been used for understanding cloud processes, global hydrologic processes, and linkages between the atmospheric and terrestrial water resources. While measurements of the isotopic composition of rainfall have been available since the 1950s, a remarkably small number of measurements of the isotopic composition of atmospheric water vapor have been made because of the challenges associated with

collecting air samples for laboratory mass spectrometric analysis [e.g., Lawrence *et al.*, 2004]. Recently, in situ methods have been applied and yielded new understanding of convective processes. Webster and Heymsfield [2003] examined isotopic composition in proximity to a convective cloud which gave new insight into the role of detrainment and cloud particles in the energy exchanges in the region of cloud systems. Lawrence *et al.* [1998, 2004] measured the isotopic depletion of boundary layer water vapor in several regions of the tropics. They found that regions with disorganized or no convection had the least isotopically depleted vapor, whereas the boundary layer vapor inside or downwind of weather systems were most depleted; this excess depletion is suggestive of an “amount effect” [Dansgaard, 1964] in which water recycled in the cloud system becomes successively depleted as the heavier isotopes are removed through precipitation. In this manner, the isotopic measurements have led to new understanding of tropospheric water vapor and clouds.

[3] To date, only two space-based instruments have been able to observe isotopic composition in the troposphere. The Atmospheric Trace Molecule Spectroscopy Experiment (ATMOS), a NASA JPL instrument, flew on the space

<sup>1</sup>Earth and Space Sciences Division, Jet Propulsion Laboratory, Pasadena, California, USA.

<sup>2</sup>PAOS and CIRES, University of Colorado, Boulder, Colorado, USA.

<sup>3</sup>Atmospheric and Environmental Research, Inc., Lexington, Massachusetts, USA.

<sup>4</sup>Department of Physics, University of Denver, Denver, Colorado, USA.

<sup>5</sup>Raytheon Information Solutions, Pasadena, California, USA.

<sup>6</sup>NASA Langley Research Center, Hampton, Virginia, USA.

<sup>7</sup>Atmospheric, Oceanic and Planetary Physics, Clarendon Laboratory, Oxford, UK.

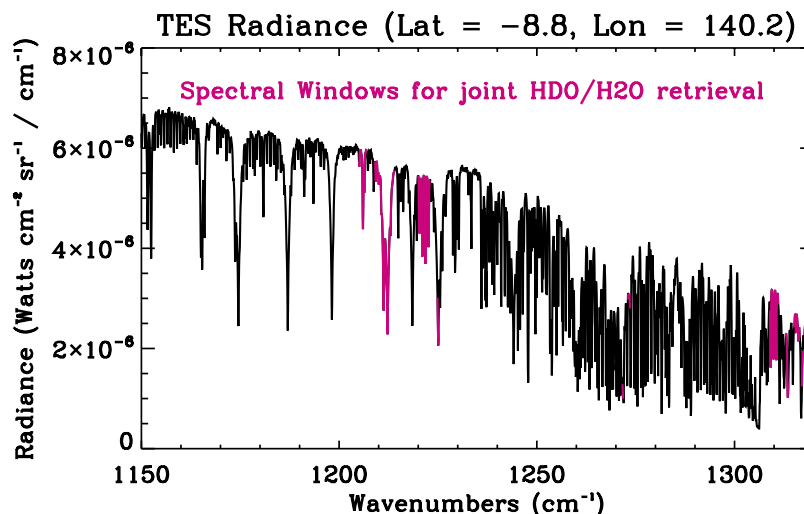


**Figure 1.** The black line shows the TES observed tropical radiance for 20 September 2004. The red lines show the spectral windows used for estimating HDO and H<sub>2</sub>O.

shuttle, and measured isotopic composition in the upper troposphere and stratosphere [Rinsland *et al.*, 1991; Irion *et al.*, 1996; Moyer *et al.*, 1996; Kuang *et al.*, 2003]. Spectra from the Interferometer for Monitoring of Greenhouse gases (IMG) on board the AD EOS-1 platform, spanning the 9 months of its operation, were used to obtain zonal climatology of midtroposphere HDO [Zakharov *et al.*, 2004]. Although limited in their spatial and temporal coverage, the data from these instruments provide strong indicators of large-scale transport, condensation, and convective processes.

[4] Here we present new measurements of the global distribution of the tropospheric HDO/H<sub>2</sub>O ratio using spectral radiances taken by the Tropospheric Emission Spectrometer (TES) [Beer *et al.*, 2001]. It is important that the estimate of the HDO/H<sub>2</sub>O ratio is robust against the spectral interference of H<sub>2</sub>O on HDO due to pressure broadening and the TES spectral resolution. Furthermore, the estimated errors must be well quantified and much smaller than the expected variability of the lower tropospheric HDO/H<sub>2</sub>O ratio of approximately 15%. This paper first discusses the approach and error characterization for estimating profiles of the HDO/H<sub>2</sub>O ratio from TES radiances. We then discuss global and regional features of TES HDO/H<sub>2</sub>O estimates for 20 September 2004; these estimates show spatial variability consistent with the underlying meteorology and illuminate the role of water vapor transport and hydrologic processes in the atmosphere. Given these results and a temporal sampling of one global survey every 2 days and an expected lifetime of 5 years, TES can provide an unprecedented global scale perspective of the tropospheric isotopic depletion of water vapor.

## 2. Overview of TES Observations

[5] The Tropospheric Emission Spectrometer is an infrared Fourier transform spectrometer (FTS) that measures the spectral infrared (IR) radiances between 650 cm<sup>-1</sup> and 3050 cm<sup>-1</sup> in a limb-viewing and a nadir (downward looking) mode. The observed IR radiance is imaged onto an array

of 16 detectors that have a combined horizontal footprint of 5.3 km by 8.4 km in the nadir viewing mode. In the nadir view, TES estimates of atmospheric distributions provide vertical information of the more abundant tropospheric species such as H<sub>2</sub>O, HDO, O<sub>3</sub>, CO, and CH<sub>4</sub> [e.g., Worden *et al.*, 2004b, and references therein]. However, sufficient spectral resolution and signal-to-noise ratio are required to distinguish between trace gas amounts at different altitudes because vertical information about trace gas concentrations is obtained only from spectral variations along the line of sight. Consequently, the TES spectral resolution was chosen to match the average pressure-broadened widths of weak infrared molecular transitions in the lower troposphere for nadir measurements (0.06 cm<sup>-1</sup> apodized) [Beer *et al.*, 2001].

[6] The first full (16 orbit) global survey from the TES occurred on 20 September 2004 and is the focus of the present study. This global survey consists of nearly 1100 nadir measurements. The ascending orbit crosses the equator at a 1400 local solar time and the descending orbit crosses the equator at 0200 local solar time. For the nadir viewing mode, the sampling along the mostly north-south orbit track is one observation every 5 degrees latitude. The orbits are spaced roughly every 22 degrees in longitude, although the nighttime and daytime orbits can overlap giving locally higher sampling density.

[7] Defining an optimal set of spectral windows for the TES estimates of the HDO/H<sub>2</sub>O ratio is critical because the radiance contribution from the HDO spectral lines typically overlap the contribution from H<sub>2</sub>O, CH<sub>4</sub>, and N<sub>2</sub>O. Figure 1 shows the radiance spectrum of a tropical scene (-8.8 degrees latitude, 140 degrees longitude) from the 20 September 2004 TES global survey for the spectral region between 1100 cm<sup>-1</sup> and 1350 cm<sup>-1</sup>. This spectral region contains many water lines that are used for TES estimates of H<sub>2</sub>O [Worden *et al.*, 2004b]. There are also many HDO lines that can be used for estimating atmospheric distributions of HDO and H<sub>2</sub>O [Toth, 1999; Rothman *et al.*, 2003]. Spectral windows are selected that maximize the information content of the estimated HDO and H<sub>2</sub>O profiles [Worden *et al.*, 2004b]. However, we also add one of the spectral windows used for the TES H<sub>2</sub>O

estimates in order to ensure consistency between the initial TES H<sub>2</sub>O estimate and the joint HDO/H<sub>2</sub>O estimate. These spectral windows are shown in Figure 1.

### 3. Estimation Theory for Simultaneous Estimate of HDO and H<sub>2</sub>O

[8] The estimation method and error characterization for the distribution of the HDO/H<sub>2</sub>O ratio uses the general methodology and error characterization from *Rodgers* [2000] and the error characterization used for simultaneous estimates of atmospheric trace gasses and temperature described by *Rodgers and Connor* [2003] and *Worden et al.* [2004b]. The approach described in this section is to jointly estimate profiles of HDO and H<sub>2</sub>O. An a priori covariance is developed which includes the expected variability of both HDO and H<sub>2</sub>O and the correlations between the two molecules; the inverse of this a priori covariance is used to constrain the joint estimate [*Rodgers*, 2000]. A critical component of the error characterization of the HDO/H<sub>2</sub>O ratio is to understand how the errors from the HDO and H<sub>2</sub>O components of the simultaneous estimate are related.

[9] A forward model can be related to a set of observations through an additive noise model:

$$\mathbf{y} = \mathbf{F}(\mathbf{x}, \mathbf{b}) + \mathbf{n} \quad (1)$$

where  $\mathbf{y} \in \mathbb{R}^N$  is the observation vector containing in this case the calibrated radiances from TES, The forward model operator,  $\mathbf{F}: \mathbb{R}^M \rightarrow \mathbb{R}^N$ , simulates a spectrum produced from the propagation of radiation through the atmosphere to the spacecraft. The vector  $\mathbf{n} \in \mathbb{R}^N$  accounts for white Gaussian noise with a zero-mean so that

$$\mathbf{S}_n = E[\mathbf{nn}^T] = \sigma^2 \mathbf{I} \quad (2)$$

where  $E[\bullet]$  is the expectation operator  $[\ ]$ ,  $\sigma^2$  is the variance of the noise and  $\mathbf{I}$  is the identity matrix. The forward model [e.g., *Clough et al.*, 2005] is a function of the “full” state vector,  $\mathbf{x} \in \mathbb{R}^M$  where  $\mathbf{x}$  is the distribution of the retrieved atmospheric gas. For example, in this study we define the full state vector  $\mathbf{x}$  as the logarithm of the volume mixing ratio (vmr) of HDO (defined as  $q_D$ ) and H<sub>2</sub>O (defined as  $q_H$ ) as a function of log pressure grid ( $P$ ). The logarithm of the volume mixing ratio is used to better constrain the estimate of HDO and H<sub>2</sub>O which can vary by orders of magnitude over a few kilometer and also constrains the estimate to be positive. In the TES forward model algorithm, the full state vector is discretized on 85 pressure levels:

$$\mathbf{x} = \begin{bmatrix} \ln q_D(P_0) \\ \downarrow \\ \ln q_D(P_{85}) \\ \ln q_H(P_0) \\ \downarrow \\ \ln q_H(P_{85}) \end{bmatrix}, \quad (3)$$

where the arrows indicate the other pressure levels between 0 and 85. The vector  $\mathbf{b}$  contains all the other parameters,

trace gases, atmospheric temperature distribution, geometry of the spacecraft, calibration, etc., necessary to define the radiance for the TES sensors. Fine discretization in the vertical computational grid is required to model accurately the radiative transfer through the atmosphere. However, because TES measurements are not sensitive to structure on this fine discretization, the estimate must be regularized. Regularization of this joint estimate includes defining a “retrieval” vector that limits the possible values of the full state vector. For this study the retrieval vector and the full state vector are related by a linear mapping:

$$\mathbf{x} = \mathbf{M}\mathbf{z} \quad (4)$$

where  $\mathbf{z} \in \mathbb{R}^M$  is the retrieval vector and  $\mathbf{M} \in \mathbb{R}^{M \times N}$  is a mapping matrix. Because the mapping used here is linear, the mapping matrix may also be interpreted as

$$\mathbf{M} = \frac{\partial \mathbf{x}}{\partial \mathbf{z}}. \quad (5)$$

The mapping matrix represents a “hard constraint” because the estimate cannot take on values outside the range space of  $\mathbf{M}$  [*Rodgers*, 2000]. We construct the map for a joint estimate of HDO and H<sub>2</sub>O:

$$\mathbf{M} = \begin{pmatrix} \mathbf{M}_{D-H} & 0 \\ 0 & \mathbf{M}_{D-H} \end{pmatrix} \quad (6)$$

where  $\mathbf{M}_{D-H}$  is a map that relates retrieval levels on a subset of the full-state pressure grid to the 85-level TES full state pressure grid using linear-in-log pressure interpolation. For these tropospheric retrievals we use 14 retrieval levels with 11 of those levels in the troposphere and three in the stratosphere.

[10] The vertical profile estimate is obtained by solving the following augmented nonlinear least squares (NLLS) solution:

$$\hat{\mathbf{x}} = \mathbf{M} \cdot \min_{\mathbf{z}} \left( \|\mathbf{y} - \mathbf{F}(\mathbf{M}\mathbf{z})\|_{\mathbf{S}_n}^2 + \|\mathbf{z} - \mathbf{z}_c\|_{\Lambda}^2 \right) \quad (7)$$

where  $\mathbf{z}_c$  is a constraint vector,  $\Lambda$  is a constraint matrix, and  $\mathbf{S}_n$  is the error covariance matrix defined in equation (2). The constraint vector and matrix are referred to as “soft” constraints because they provide a priori information about the solution space, e.g., smoothness of the profile or statistical distribution of the state vector, without restricting that solution space for the estimate. The nonlinear estimate of the HDO and H<sub>2</sub>O atmospheric concentrations is based on the iterative minimization of the observed nadir viewing radiances with the forward model evaluated at successive estimates of the retrieval vector. The convergence criteria is based on a combination of metrics that include the derivative of the cost function, as described by equation (7), change in the state parameters, and the change in the cost function [*Bowman et al.*, 2006].

#### 3.1. Error Characterization for Simultaneous Estimate

[11] If the estimate is “close” to the true state, then its dependence on the choice of constraint vector, constraint

matrix, and true state can be described by the linear estimate [Rodgers, 2000]

$$\hat{\mathbf{x}} = \mathbf{x}_a + \mathbf{A}_{xx}(\mathbf{x} - \mathbf{x}_a) + \mathbf{M}\mathbf{G}_z\mathbf{n} + \mathbf{M}\mathbf{G}_z \sum_i \mathbf{K}_i(\mathbf{b}_i - \mathbf{b}_i^a), \quad (8)$$

where  $\mathbf{M}$  is the mapping matrix,  $\mathbf{A}_{xx}$  is the averaging kernel matrix,  $\mathbf{n}$  is the noise vector,  $\mathbf{x}$  is the “true” full state vector (the HDO and H<sub>2</sub>O profiles),  $\mathbf{x}_a = \mathbf{M}\mathbf{z}_a$  is the constraint state vector,  $\mathbf{G}_z$  is the gain matrix, which is defined by:

$$\mathbf{G}_z = \frac{\partial \mathbf{z}}{\partial \mathbf{F}} = (\mathbf{K}_z^T \mathbf{S}_n^{-1} \mathbf{K}_z + \Lambda_z)^{-1} \mathbf{K}_z^T \mathbf{S}_n^{-1}. \quad (9)$$

The Jacobian,  $\mathbf{K}_z$ , is defined by

$$\mathbf{K}_z = \frac{\partial \mathbf{F}}{\partial \mathbf{x}} \frac{\partial \mathbf{x}}{\partial \mathbf{z}} = \mathbf{K}_x \mathbf{M}. \quad (10)$$

The last term in equation (8) refers to the sum (subscript  $i$ ) over all parameters (denoted by  $\mathbf{b}$ ) that contribute error to the estimate.

[12] Equation (8) is a valid approximation to equation (7) when

$$\mathbf{K}_x(\mathbf{x} - \hat{\mathbf{x}}) \approx \mathbf{F}(\mathbf{x}, \mathbf{b}) - \mathbf{F}(\hat{\mathbf{x}}, \mathbf{b}), \quad (11)$$

where the forward model  $\mathbf{F}$  is defined in equation (1).

[13] The averaging kernel matrix, termed the resolution matrix by Parker [1994],  $\mathbf{A}_{xx} = \partial \hat{\mathbf{x}} / \partial \mathbf{x}$ , is the sensitivity of the estimate to the true state of the atmosphere [Rodgers, 2000] and is computed as

$$\mathbf{A}_{xx} = \frac{\partial \hat{\mathbf{x}}}{\partial \mathbf{x}} = \frac{\partial \hat{\mathbf{x}}}{\partial \mathbf{z}} \frac{\partial \mathbf{z}}{\partial \mathbf{F}} \frac{\partial \mathbf{F}}{\partial \mathbf{x}} = \mathbf{M}\mathbf{G}_z\mathbf{K}_x. \quad (12)$$

Estimates of HDO and H<sub>2</sub>O will be sensitive to different parts of the atmosphere and also be correlated with each other; consequently, we must develop an error analysis which accounts for these different sensitivities and correlations when constructing the ratio of the two profiles. A first step in developing this error characterization is to subdivide the averaging kernel and gain matrices:

$$\mathbf{A}_{xx} = \begin{pmatrix} \mathbf{A}_{DD} & \mathbf{A}_{DH} \\ \mathbf{A}_{HD} & \mathbf{A}_{HH} \end{pmatrix}, \quad (13)$$

where the averaging kernel with subscript DD refers to derivative of the estimated state of HDO with respect to the true state of HDO and DH refers to the derivative of the estimated state of HDO with respect to the true state of H<sub>2</sub>O. The averaging kernels with subscripts HH and HD are defined analogously. Similarly, the gain matrix can be subdivided into two submatrices:

$$\mathbf{G}_z = \begin{bmatrix} \mathbf{G}_z^D \\ \mathbf{G}_z^H \end{bmatrix} \quad (14)$$

[14] The error in the estimate of the atmospheric profile is the true state minus the estimate:

$$\tilde{\mathbf{x}} = \mathbf{x} - \hat{\mathbf{x}} \quad (15)$$

Substituting equation (8) into equation (15) leads to

$$\tilde{\mathbf{x}} = \underbrace{(\mathbf{I} - \mathbf{A}_{xx})(\mathbf{x} - \mathbf{x}_a)}_{\text{smoothing error}} + \underbrace{\mathbf{M}\mathbf{G}_z\mathbf{n}}_{\text{noise error}} + \underbrace{\mathbf{M}\mathbf{G}_z \sum_i \mathbf{K}_i(\mathbf{b}_i - \mathbf{b}_i^a)}_{\text{model error}} \quad (16)$$

The second term on the right-hand side transforms the random spectral error to an error on the full state vector. The third term transforms errors in those parameters which affect the estimate of HDO and H<sub>2</sub>O, such as uncertainty in either a previously retrieved or a priori profile of atmospheric temperature or calibration to an error on the full state vector. The first term, the so-called “smoothing” error [Rodgers, 2000], results from applying constraints on the estimate of HDO and H<sub>2</sub>O and is of special concern. These constraints can be a combination of “hard” constraints (e.g., representing the profile on a coarse pressure grid) or “soft” constraints (e.g., subjectively adding a quadratic penalty function in equation (9) to ensure an acceptable regularization). Physically, the smoothing error describes the extent to which a remote observing system is sensitive to fine structure as defined, in this context, on the forward model grid.

[15] The total error covariance matrix is defined as

$$\mathbf{S}_{\tilde{\mathbf{x}}} = E[(\tilde{\mathbf{x}} - \bar{\tilde{\mathbf{x}}})(\tilde{\mathbf{x}} - \bar{\tilde{\mathbf{x}}})^T], \quad (17)$$

where  $\bar{\tilde{\mathbf{x}}}$  is the mean of  $\tilde{\mathbf{x}}$  from equation (15). Substituting equation (16) into equation (17) leads to the following:

$$\begin{aligned} \mathbf{S}_{\tilde{\mathbf{x}}} &= (\mathbf{A}_{xx} - \mathbf{I})\mathbf{S}_a(\mathbf{A}_{xx} - \mathbf{I})^T + \mathbf{M}\mathbf{G}_z\mathbf{S}_n\mathbf{G}_z^T\mathbf{M}^T \\ &+ \mathbf{M}\mathbf{G}_z \left( \sum_i \mathbf{K}_i \mathbf{S}_i^j \mathbf{K}_i^T \right) (\mathbf{M}\mathbf{G}_z)^T \end{aligned} \quad (18)$$

where  $\bar{\tilde{\mathbf{x}}} = E[\tilde{\mathbf{x}}]$ , and  $\mathbf{S}_a = E[(\mathbf{x} - \bar{\mathbf{x}})(\mathbf{x} - \bar{\mathbf{x}})^T]$ . The smoothing error covariance matrix is composed of the averaging kernel matrix and the covariance of the state vector. Hence the smoothing error will decrease as the resolution of the estimate increases, i.e., the averaging kernel matrix will approximate the identity matrix or if there is little variance in the state vector.

[16] As discussed earlier, the full-state vector is defined as the logarithm of the mixing ratio. Using the logarithm also facilitates the error characterization for the ratio; the log of the HDO/H<sub>2</sub>O ratio is a construction of the log of HDO and H<sub>2</sub>O, i.e.,

$$\mathbf{x}_R = \ln \frac{\mathbf{q}_D}{\mathbf{q}_H} = \mathbf{x}_D - \mathbf{x}_H \quad (19)$$

The a priori covariance used for constraining the estimate of HDO and H<sub>2</sub>O, and evaluating the smoothing error,  $\mathbf{S}_a = E[(\mathbf{x} - \bar{\mathbf{x}})(\mathbf{x} - \bar{\mathbf{x}})^T]$ , is

$$\mathbf{S}_a = \begin{bmatrix} E[(\mathbf{x}_D - \bar{\mathbf{x}}_D)(\mathbf{x}_D - \bar{\mathbf{x}}_D)^T] & E[(\mathbf{x}_D - \bar{\mathbf{x}}_D)(\mathbf{x}_H - \bar{\mathbf{x}}_H)^T] \\ E[(\mathbf{x}_H - \bar{\mathbf{x}}_H)(\mathbf{x}_D - \bar{\mathbf{x}}_D)^T] & E[(\mathbf{x}_H - \bar{\mathbf{x}}_H)(\mathbf{x}_H - \bar{\mathbf{x}}_H)^T] \end{bmatrix} \quad (20)$$

If we set  $\mathbf{x}_D = \mathbf{x}_R + \mathbf{x}_H$ , and we specify that  $E[(\mathbf{x}_H - \bar{\mathbf{x}}_H)(\mathbf{x}_R - \bar{\mathbf{x}}_R)^T] = 0$ , that is, the atmospheric water content is uncorrelated with the fractionation, then equation (20) becomes

$$\mathbf{S}_a = \begin{bmatrix} \mathbf{S}_a^H + \mathbf{S}_a^R & \mathbf{S}_a^H \\ \mathbf{S}_a^H & \mathbf{S}_a^H \end{bmatrix} \quad (21)$$

where  $\mathbf{S}_H$  is the a priori covariance for H<sub>2</sub>O and  $\mathbf{S}_R$  is the a priori covariance for the log of the fractionation. For TES estimates of the HDO and H<sub>2</sub>O distributions, the a priori covariance for water,  $\mathbf{S}_H$ , is constructed using the MOZART [Brasseur et al., 1998; Horowitz et al., 2003] model but scaled to the expected uncertainty of NCEP water content predictions [Worden et al., 2004b]. The a priori statistics for  $\mathbf{S}_R$  is based on a version of the National Center for Atmospheric Research (NCAR) Community Atmosphere Model (CAM) [e.g., Collins et al., 2004] that has been modified to predict the isotopic composition of water using the approach developed by Noone and Simmonds [2002]. The inverse of this a priori covariance is used as the constraint matrix in equation (9). The a priori covariance and constraints used for the estimate could be further improved by augmenting the cross terms of equation (21) with known (a priori) correlations between water amount and the isotopic distribution of water. However, we choose not to include these additional cross terms as they are challenging to calculate and will probably not improve greatly on the convergence or subsequent characterization of the optimal estimate. A consequence of not including these correlations is that we will overestimate the errors.

### 3.2. Error Characterization of HDO to H<sub>2</sub>O Ratio

[17] Now that the averaging kernel, gain, and a priori constraint matrices are defined for a joint estimate of HDO and H<sub>2</sub>O we can now derive the error covariance matrices for the ratio; these covariance matrices are critical for defining the science that can be addressed with these estimates of the HDO/H<sub>2</sub>O ratio.

[18] From the simultaneous estimate of HDO and H<sub>2</sub>O we can construct the ratio:

$$\hat{\mathbf{x}}_R = \log \frac{\hat{q}_D}{\hat{q}_H} = \hat{\mathbf{x}}_D - \hat{\mathbf{x}}_H, \quad (22)$$

where, recall from equation (3), that the mixing ratios of HDO and H<sub>2</sub>O are defined by  $q_D$  and  $q_H$  but the retrieval is performed using the logarithm of these quantities. In order to derive the error covariance and averaging kernel matrices for equation (22), we first define the linear estimate for  $\hat{\mathbf{x}}_D$  and  $\hat{\mathbf{x}}_H$  separately under the assumption that HDO and H<sub>2</sub>O are jointly retrieved:

$$\hat{\mathbf{x}}_D = \mathbf{x}_a^D + \mathbf{A}_{DD}(\mathbf{x}_D - \mathbf{x}_a^D) + \mathbf{A}_{DH}(\mathbf{x}_H - \mathbf{x}_a^H) + \mathbf{M}_{D-H}\mathbf{G}_z^D \mathbf{n} + \mathbf{M}_{D-H}\mathbf{G}_z^D \sum_i \mathbf{K}_i^b (\mathbf{b}_i - \mathbf{b}_i^a) \quad (23)$$

and

$$\hat{\mathbf{x}}_H = \mathbf{x}_a^H + \mathbf{A}_{HH}(\mathbf{x}_H - \mathbf{x}_a^H) + \mathbf{A}_{HD}(\mathbf{x}_D - \mathbf{x}_a^D) + \mathbf{M}_{D-H}\mathbf{G}_z^H \mathbf{n} + \mathbf{M}_{D-H}\mathbf{G}_z^H \sum_i \mathbf{K}_i^b (\mathbf{b}_i - \mathbf{b}_i^a) \quad (24)$$

where the different components of the averaging kernel and gain matrix are defined in equations (13) and (14), respectively. Note how the estimate of H<sub>2</sub>O (denoted by  $H$ ) affects the estimate of HDO (denoted by  $D$ ) through the off-diagonal blocks of the averaging kernel and vice versa. Using equations (23) and (24), equation (22) becomes:

$$\hat{\mathbf{x}}_R = \mathbf{x}_a^R + (\mathbf{A}_{DD} - \mathbf{A}_{HD})(\mathbf{x}_D - \mathbf{x}_a^D) - (\mathbf{A}_{HH} - \mathbf{A}_{DH})(\mathbf{x}_H - \mathbf{x}_a^H) + \mathbf{G}_R \mathbf{n} + \mathbf{G}_R \sum_i \mathbf{K}_i^b (\mathbf{b}_i - \mathbf{b}_i^a), \quad (25)$$

where  $\mathbf{x}_a^R = \mathbf{x}_a^D - \mathbf{x}_a^H$ , and  $\mathbf{G}_R = \mathbf{M}_{D-H}(\mathbf{G}_z^D - \mathbf{G}_z^H)$ .

[19] The total error for the estimate of the fractionation is constructed in the same manner as in equations (16) through (18), except that the smoothing error must account for the correlations between HDO and H<sub>2</sub>O:

$$\begin{aligned} \mathbf{S}_* &= (\mathbf{A}_{DD} - \mathbf{A}_{HD} - \mathbf{I})\mathbf{S}_{DD}(\mathbf{A}_{DD} - \mathbf{A}_{HD} - \mathbf{I})^T \\ &+ (\mathbf{A}_{HH} - \mathbf{A}_{DH} - \mathbf{I})\mathbf{S}_{HH}(\mathbf{A}_{HH} - \mathbf{A}_{DH} - \mathbf{I})^T \\ &- (\mathbf{A}_{DD} - \mathbf{A}_{HD} - \mathbf{I})\mathbf{S}_{DH}(\mathbf{A}_{HH} - \mathbf{A}_{DH} - \mathbf{I})^T \\ &- (\mathbf{A}_{HH} - \mathbf{A}_{DH} - \mathbf{I})\mathbf{S}_{HD}(\mathbf{A}_{DD} - \mathbf{A}_{HD} - \mathbf{I})^T \\ &+ \mathbf{G}_R \mathbf{S}_n \mathbf{G}_R^T + \mathbf{G}_R \left( \sum_i \mathbf{K}_i \mathbf{S}_i^b \mathbf{K}_i^T \right) \mathbf{G}_R^T \end{aligned} \quad (26)$$

where  $\mathbf{S}_{DD}$ ,  $\mathbf{S}_{HH}$ ,  $\mathbf{S}_{DH}$ ,  $\mathbf{S}_{HD}$  are the submatrix elements of the a priori covariance for the joint estimate of HDO and H<sub>2</sub>O. On the basis of the assumptions described by equation (20), these submatrices are

$$\begin{aligned} \mathbf{S}_{DD} &= \mathbf{S}_a^H + \mathbf{S}_a^R \\ \mathbf{S}_{HH} &= \mathbf{S}_a^H \\ \mathbf{S}_{DH} &= \mathbf{S}_a^H \\ \mathbf{S}_{HD} &= \mathbf{S}_a^H, \end{aligned} \quad (27)$$

[20] Inspection of equations (25) and (26) underscore the utility of retrieving HDO jointly with H<sub>2</sub>O. The second line of equation (26) is subtracted from the first line and the gain matrix for water is subtracted from the gain matrix for HDO resulting in some error cancellation in the smoothing, measurement, and model parameter error components. If HDO estimate had occurred after the H<sub>2</sub>O estimate and the ratio subsequently constructed, the error for the ratio would contain additive errors from both H<sub>2</sub>O and HDO and as expected the total resulting error would be larger than from the joint estimate. If the spectral absorption lines from HDO and H<sub>2</sub>O did not significantly overlap, this additive error would be small; however, since almost all the HDO lines spectrally overlap for this viewing mode with the H<sub>2</sub>O lines, it is critical to use this joint estimation approach for inferring the HDO/H<sub>2</sub>O ratio.

## 4. TES Estimates of the HDO/H<sub>2</sub>O Ratio

### 4.1. Error Characteristics

[21] The TES Level 2 algorithm performs estimates of the atmospheric and surface temperature, water, cloud properties, ozone, and if the observation is over land, surface

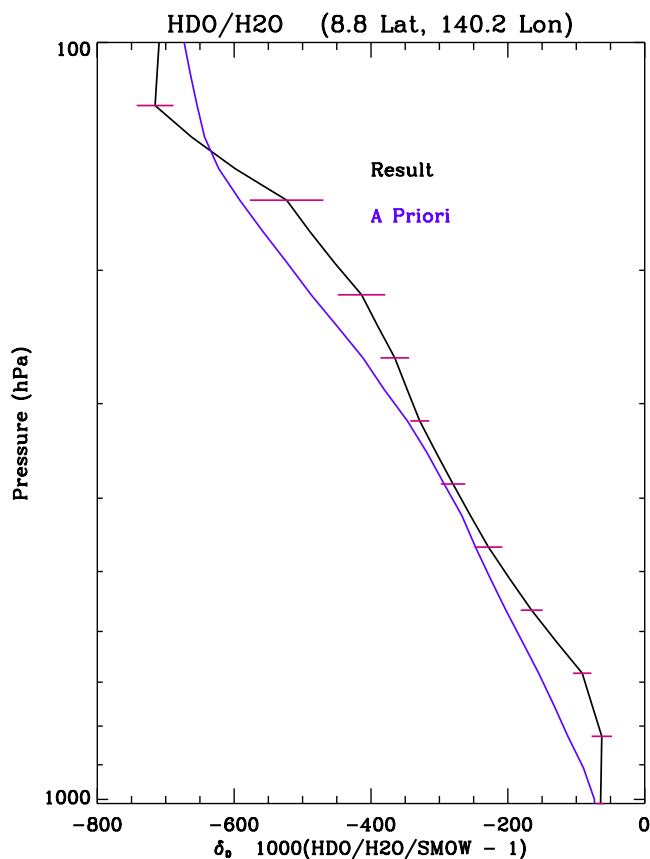


**Figure 2.** The HDO/H<sub>2</sub>O estimate using the radiance from Figure 1. The blue line is the a priori profile used to constrain the estimate, the black line is the estimate, and the red dashes are the calculated error bars. Note that the error bars do not indicate the altitude region where the TES retrieval is sensitive.

emissivity. These quantities are then fixed for the subsequent estimate of HDO and H<sub>2</sub>O. The initial guess for HDO for all profiles is set to this TES estimated H<sub>2</sub>O atmospheric profile multiplied by a single a priori profile of the HDO/H<sub>2</sub>O ratio calculated from a run of the NCAR CAM augmented with isotopic physics. However, we treat the initial guess and the a priori separately in order to simplify the error characterization. Consequently, the a priori profile for HDO is the product of the a priori profile of H<sub>2</sub>O and the a priori profile of the HDO/H<sub>2</sub>O ratio. Another choice used in the estimation of the HDO/H<sub>2</sub>O ratio is to use only a single a priori profile of the HDO/H<sub>2</sub>O ratio for all observations. This choice of using a single a priori profile for the HDO/H<sub>2</sub>O ratio is not optimal for the higher latitudes where it is expected that there is much less HDO relative to H<sub>2</sub>O. Consequently, the estimate of the HDO/H<sub>2</sub>O ratio will be biased at higher latitude to the equatorial a priori when the estimate has little sensitivity to the true state. On the other hand, use of a single a priori allows for a simpler analysis of the latitudinal and longitudinal distribution of the HDO/H<sub>2</sub>O ratio as changes in the a priori do not have to be explicitly accounted for in an analysis.

[22] An estimate of the HDO/H<sub>2</sub>O ratio using the observed radiance and spectral windows from Figure 1 are

shown in Figure 2. The retrieved ratio is given in the usual  $\delta_D$  (or parts per thousand) notation following the definition

$$\delta_D = 1000 \times \left( \frac{q_{\text{HDO}}/q_{\text{H}_2\text{O}}}{R_{\text{SMOW}}} - 1 \right), \quad (28)$$

where  $R_{\text{SMOW}}$  is the isotope ratio of Vienna Standard Mean Ocean Water and is defined to be  $R_{\text{SMOW}} = 3.1 \times 10^{-4}$  by volume. The error bars shown in Figure 2 are the diagonal of the root mean squared (RMS) of the total error; the total error includes the smoothing error, measurement error, and systematic error from the prior temperature retrieval. This retrieved profile shows, at least for this tropical region, more isotopically depleted water vapor in the upper troposphere relative to the lower troposphere.

[23] The RMS of the diagonal of the different error covariances are shown in Figure 3 as a function of pressure between surface and 100 hPa. The total error is the sum of the following:

[24] 1. The smoothing error (the dominant error for this pressure grid).

[25] 2. The measurement error, which is taken to be the calculated NESR but multiplied by 0.67 to account for apodization. Note that we do not include a correction to the

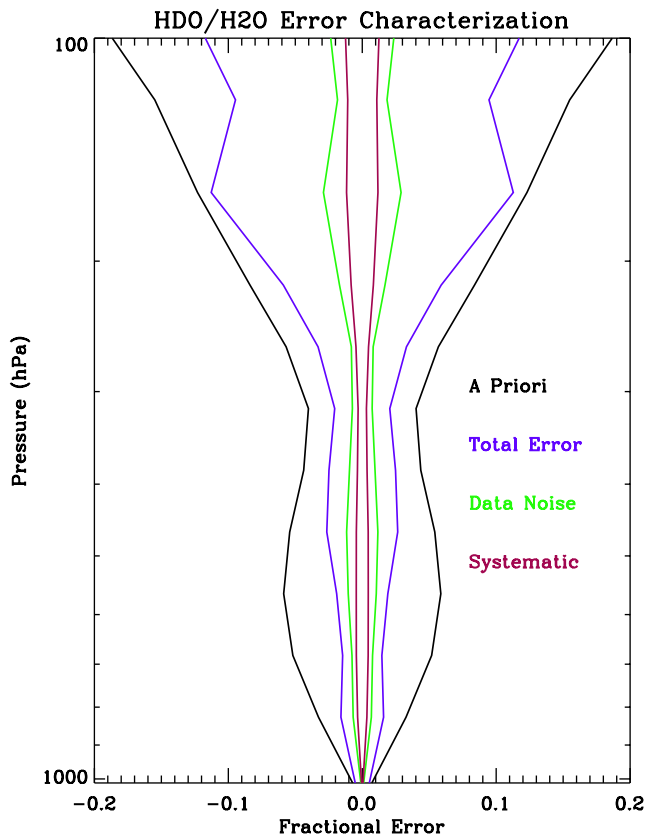


**Figure 3.** The a priori error is computed using a tropical covariance from the NCAR CAM for the HDO/H<sub>2</sub>O ratio and the a priori covariance for water discussed by Worden *et al.* [2004a, 2004b]. The total error is the sum of the smoothing error, measurement error (data noise) and systematic errors from temperature and clouds (and surface emissivity if over land).

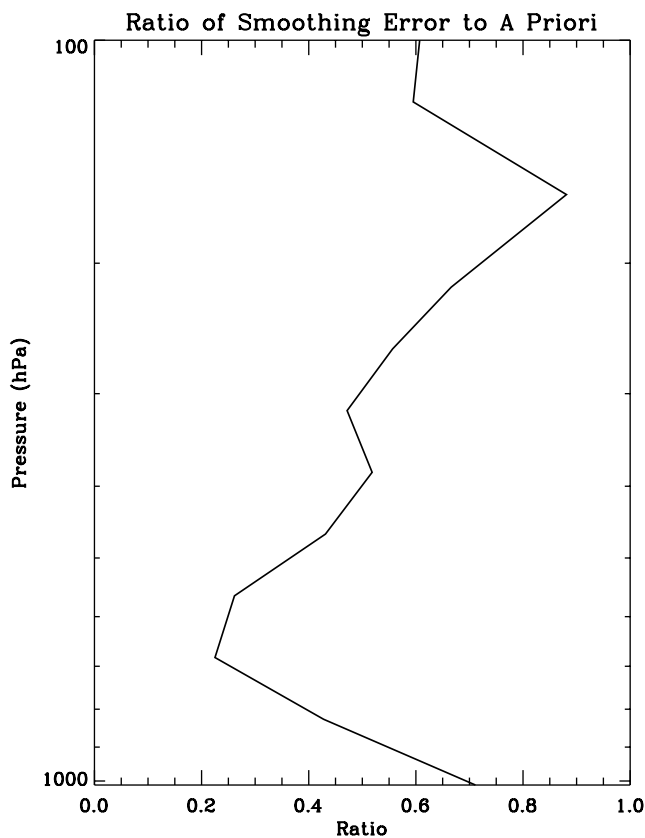


**Figure 4.** The ratio of the square-root of the diagonals of the smoothing error covariance and the square-root of the diagonals of the a priori covariance. Most of the reduction in error is at 700 hPa.

total error analysis due to smoothing of spectral elements resulting from apodization because of the difficulty in inverting a large measurement error covariance matrix and because we find that this correction is negligible.

[26] 3. Error from the prior estimate of temperature, clouds, surface temperature, and also surface emissivity if the retrieval is taken over land.

[27] For this retrieval the error from noise and systematic error amounts to approximately 1% near 700 hPa. We do not include spectroscopic line strength errors in equation (26) but examine those separately later in this paper.

[28] The smoothing error in Figure 3 is the component of error due to unresolved fine structure on the reported pressure grid. Evaluation of the smoothing error depends on the choice of a priori statistics for the true state of the atmosphere. The calculated smoothing is based on a tropical climatology from the isotopic version of the NCAR-CAM. We compare the calculated smoothing error of each retrieval with the a priori covariance in order to determine if the estimate is sensitive to the true distribution of the HDO/H<sub>2</sub>O ratio. Normally, an averaging kernel matrix would be used to examine the sensitivity of an estimate to perturbations in the true state; however, an explicit averaging kernel matrix of the estimated HDO/H<sub>2</sub>O ratio to the true state of the HDO/H<sub>2</sub>O ratio cannot be defined because different combinations of HDO and H<sub>2</sub>O perturbations can give similar values for perturbations in the estimated ratio. Therefore we

examine the ratio of the diagonal of the smoothing error to the diagonal of the a priori covariance in order to determine the altitude region where the estimate of the HDO/H<sub>2</sub>O ratio is sensitive (Figure 4). Figure 4 shows that the estimated HDO/H<sub>2</sub>O ratio is primarily sensitive to the true distribution of the HDO/H<sub>2</sub>O ratio between 850 hPa and 300 hPa with peak sensitivity at around 700 hPa. We find this sensitivity (or reduction in error) will vary with temperature, clouds, and water amount.

#### 4.2. Global Characterization of TES HDO/H<sub>2</sub>O Estimates

[29] In order to show the global distribution of TES estimates of the HDO/H<sub>2</sub>O ratio, we select those retrievals where (1) converged, that is, the difference between the forward model and observed radiance is comparable to the NESR. (2) The estimate for water from is within the expected uncertainty of the estimate from the initial retrieval of temperature and water, and (3) the estimated HDO/H<sub>2</sub>O ratio is found to be sufficiently sensitive to the actual distribution of the HDO/H<sub>2</sub>O ratio. The metric used to determine sensitivity is the reduction in error between the a priori covariance and the smoothing error:

$$\mathbf{H} = \frac{1}{2}(\log_2 |\mathbf{S}_a| - \log_2 |\mathbf{S}_{\text{smooth}}|). \quad (29)$$

This equation is equivalent to the information content [Rodgers, 2000] if the smoothing error is replaced by the total error of the estimate given by equation (26). The calculated values for this form of the information content is given in terms of “bits”; each bit represents a factor of two reduction in the error “volume” described here by the a priori covariance. In principle, the information content should include all the errors described by equation (26); however, we only include the smoothing error because some of our estimates of the HDO/H<sub>2</sub>O ratio can be sensitive to the actual distribution of the HDO/H<sub>2</sub>O ratio but have an increase in the estimated uncertainty because of our nonoptimal choice for the a priori covariance; these cases tend to be at the higher latitudes as discussed in the beginning of section 4.1. For examining the global distribution of the HDO/H<sub>2</sub>O ratio we choose those estimates which have at least two bits as given by equation 29.

[30] Figure 5 shows these selected estimates linearly interpolated to a 2.5 degree longitude by 2.5 degree latitude grid. The symbols on this figure mark the location of the TES retrievals. A result that is apparent from this single global survey is the “latitude effect” in which the isotopic depletion of water vapor is larger at the higher latitudes than at the equator due to the continual rain-out of the heavier nuclides during poleward transit into an environment with lower temperature [e.g., Dansgaard, 1964]. The latitude effect is also apparent in Figure 6 in which the tropospheric average from Figure 5 is plotted as a function of latitude. Regional variations are also apparent in Figure 5 and are discussed in a subsequent paper.

[31] The estimated error for the tropospheric average shown in Figures 5 and 6 is shown in Figure 7. The error includes the smoothing error, measurement error (from the estimated NESR), and uncertainties in the prior estimate of

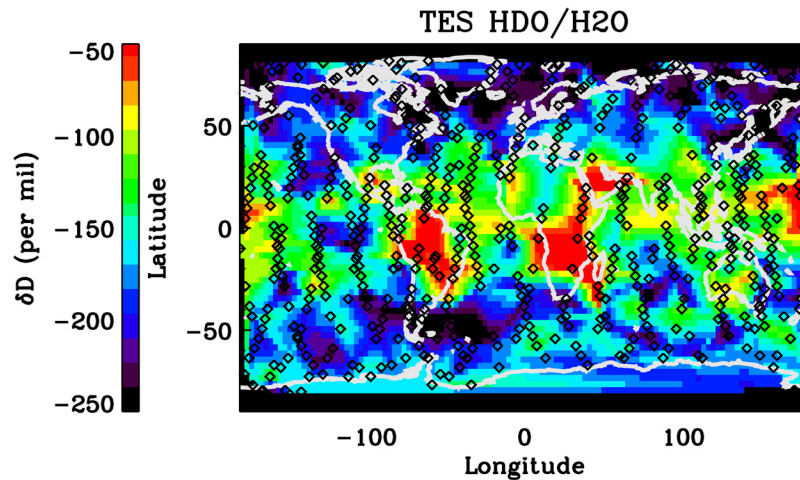


**Figure 5.** Each TES estimate of the HDO/H<sub>2</sub>O ratio is averaged between the surface and 550 hPa and then linearly interpolated onto a map with a 2.5 by 2.5 degree grid. The diamonds show the location of the TES retrievals. The map shows the “latitude” effect in which water vapor becomes more depleted at higher latitudes.

surface and atmospheric temperature and surface emissivity if the estimate is over land. The errors range from approximately 1% in the tropics (or about 8 parts per thousand) to approximately 2% in the high northern latitudes (or about 20 parts per thousand).

## 5. Comparisons to Prior Measurements and Models

[32] Few measurements of the isotopic distribution of water vapor exist in the lower troposphere because of the challenges of collecting and analyzing in situ vapor measurements [e.g., Lawrence *et al.*, 1998, 2004]. Lawrence *et al.* [2004] analyzed boundary layer vapor measurements of

the HDO/H<sub>2</sub>O ratio and found typical values of approximately  $-80$   $\delta D$  at various tropical stations when there were no storms and lower  $\delta D$  values during passage of a hurricane through the region. Figure 6 shows that TES observations of the lower tropospheric average of this ratio ranges between  $-40$   $\delta D$  and  $-170$   $\delta D$  (using equation (28) to convert between the ratio of HDO and H<sub>2</sub>O concentrations to parts per thousand relative to SMOW or  $\delta D$ ). If we assume that  $-80$   $\delta D$  is an upper bound for the isotopic composition of tropical water vapor, then there could be a bias in our observations of up to 4%.

[33] Another comparison can be made between the tropical lower tropospheric average of the HDO/H<sub>2</sub>O ratio shown in Figure 6 and the a priori profile used to constrain

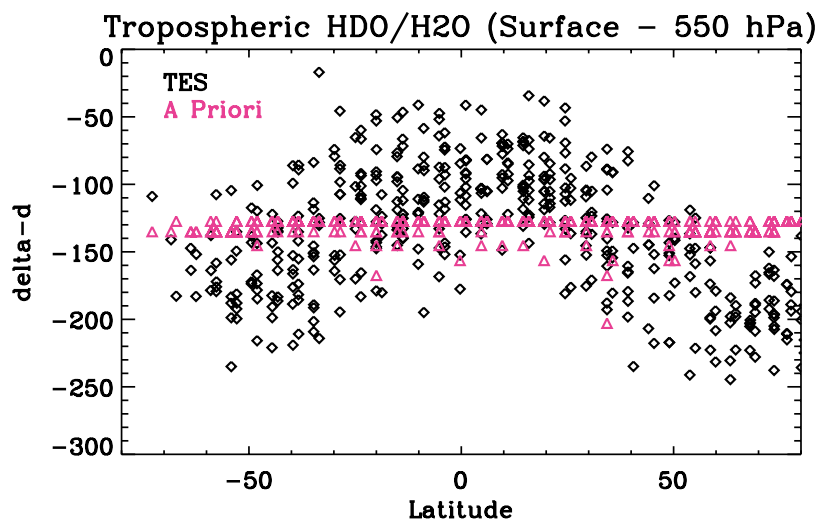


**Figure 6.** The latitudinal distribution of the HDO/H<sub>2</sub>O ratio. The black diamonds are the TES estimates of the HDO/H<sub>2</sub>O ratio (in units of delta-d) averaged between the surface and 550 hPa. The triangles show the a priori profile. A single a priori profile for the HDO/H<sub>2</sub>O ratio is used for all observations; the slight variations in a priori are due to variations in the surface pressure.

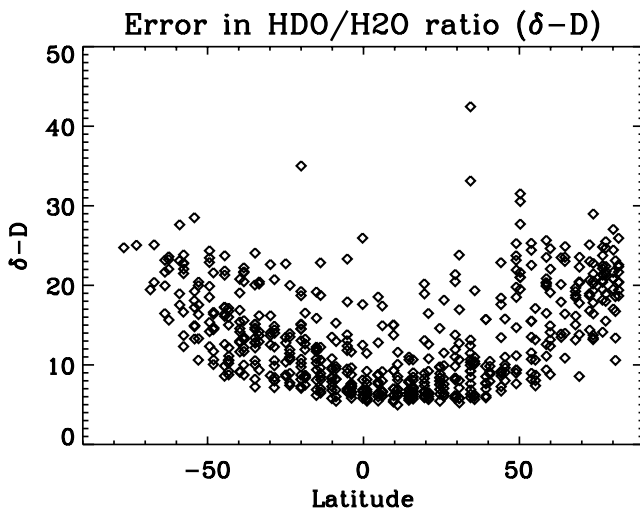


**Figure 7.** The total error for the tropospheric averages shown in Figure 6 are shown in Figure 8 in terms of  $\delta$ -D. The variation of errors is due to the variation in surface and atmospheric temperature as in Figure 7.

the estimate. As discussed in section 3, the a priori profile is calculated by averaging over all tropical profiles (between 30 degrees south and 30 degrees north) from one day of model fields from the NCAR CAM augmented with isotopic physics. This average tropospheric value of the a priori profile between the surface and 550 hPa is also shown in Figure 6 and is approximately  $-135$   $\delta$ D. This average is approximately 4% below the mean of the TES observed distribution at tropical latitudes of approximately  $-90$   $\delta$ D, which is consistent with the bias suggested by the comparison with the *Lawrence et al.* [2004] data.

[34] *Webster and Heymsfeld* [2003] also measured lower tropospheric water and HDO in both liquid and vapor phases. Their measured distributions of the HDO/H<sub>2</sub>O ratio for the lower troposphere are consistent with the distribution of HDO/H<sub>2</sub>O observed by TES. However, the spectral region used by *Webster and Heymsfeld* [2004] is similar to that used by TES for making HDO measurements. So any spectroscopic bias in the TES measurements is expected in the Webster and Heymsfeld observations. Subsequent to the Webster and Heymsfeld observations, C. Webster (private communication, 2004) used mass spectrometry to determine the vapor content of HDO above a liquid sample with a known value of the HDO/H<sub>2</sub>O ratio. Webster found a possible bias between 5% and 10% by comparing the HDO expected in the vapor with the HDO expected using the *Toth* [1999] spectroscopic line parameters. This range of 5% to 10% is consistent with the possible bias of approximately 4% suggested by comparisons to the *Lawrence et al.* [2004] data and the NCAR model. Examination of equation (28) shows that a 5% bias in the estimated HDO concentrations result in an approximately 50  $\delta$ D bias error for values of  $\delta$ D near 0 but a much smaller bias error for  $\delta$ D values much less than 0.

[35] A high priority for better characterizing TES estimates of the HDO/H<sub>2</sub>O ratio is to check the accuracy of the HDO spectroscopic line strengths (R. Toth, private communication, 2004). However, we note that while a bias may

exist in the data, this bias does not substantially affect the analysis of the relative distribution of HDO/H<sub>2</sub>O.

## 6. Conclusion

[36] We describe our methodology and corresponding error characterization for estimates of the tropospheric HDO/H<sub>2</sub>O ratio using nadir-viewed radiances from the Tropospheric Emission Spectrometer. These estimates are most sensitive in the lower troposphere near 700 hPa with decreasing sensitivity to the ratio with increasing altitude. The sensitivity to the HDO/H<sub>2</sub>O ratio also depends on temperature, water amount, and cloud conditions. Consequently, estimated values of the HDO/H<sub>2</sub>O ratio have the least uncertainty in the tropics and higher uncertainties at the higher latitudes.

[37] A possible bias of approximately 5% is suspected in the TES estimates of HDO, likely associated with the HDO spectroscopic line strengths. Should such a bias be confirmed with additional observations, a simple correction can be applied in future TES retrievals of the HDO/H<sub>2</sub>O ratio. We note that analysis of the relative distribution of the HDO/H<sub>2</sub>O ratio is less affected by this possible bias than analysis of the absolute values for any given profile.

[38] Analysis of TES retrievals of the HDO/H<sub>2</sub>O ratio needs to consider the bias associated with the a priori constraint and correlations between the HDO and H<sub>2</sub>O components of the estimate as seen in the averaging kernel matrix [e.g., *Rodgers*, 2000]. Techniques that account for this bias, cross-correlations, and error characteristics were discussed in this paper and are also shown for other TES estimates of atmospheric distributions in the works of *Bowman et al.* [2002], *Worden et al.* [2004a], *Jones et al.* [2003], and *Worden et al.* [2004b].

[39] Despite the challenges with estimating the tropospheric HDO/H<sub>2</sub>O ratio, TES observations are able to capture expected spatial distributions such as the latitude effect (more depletion of heavier water vapor isotopes at higher latitudes) and more depletion of heavier water vapor isotopes at higher altitudes [*Dansgaard*, 1964]. Regional variations are also apparent in this first TES global survey of the HDO/H<sub>2</sub>O ratio and are the focus of continuing examination.

[40] **Acknowledgments.** The authors would like to thank Christopher Webster and William Read at JPL for discussion regarding the TES HDO data and to Thomas von Clarmann for an excellent review of the manuscript. The research described in this paper was carried out at the Jet Propulsion Laboratory, California Institute of Technology, under a contract with the National Aeronautics and Space Administration.

## References

- Beer, R., T. A. Glavich, and D. M. Rider (2001), Tropospheric emission spectrometer for the Earth Observing System's Aura Satellite, *Appl. Opt.*, **40**(15), 2356–2367.
- Bowman, K. W., et al. (2006), Tropospheric emission spectrometer: Retrieval method and error analysis, *IEEE Trans. Geosci. Remote Sens.*, **44**, 1297–1307.
- Brasseur, G. P., D. A. Hauglustaine, S. Walters, P. J. Rasch, J. F. Muller, C. Granier, and X. X. Tie (1998), MOZART, a global chemical transport model for ozone and related chemical tracers: 1. Model description, *J. Geophys. Res.*, **103**(D21), 28,265–28,289.
- Clough, S. A., et al. (2005), Forward model and Jacobians for tropospheric emission spectrometer retrievals, *IEEE Trans. Geosci. Remote Sens.*, **44**, 1308–1323.

- Collins, W. D., et al. (2004), Description of the NCAR Community Atmosphere Model (CAM 3.0), *Tech. Rep. NCAR/TN-464+STR*, 210 pp., Natl. Cent. for Atmos. Res., Boulder, Colo.
- Dansgaard, W. (1964), Stable isotopes in precipitation, *Tellus*, 16(4), 436–468.
- Horowitz, L., et al. (2003), A global simulation of tropospheric ozone and related tracers: Description and evaluation of MOZART, version 2, *J. Geophys. Res.*, 108(D24), 4784, doi:10.1029/2002JD002853.
- Irion, F. W., et al. (1996), Stratospheric observations of CH<sub>3</sub>D and HDO from ATMOS Infrared solar spectra: Enrichments of deuterium in methane and implications for HD, *Geophys. Res. Lett.*, 23, 2381–2384.
- Jones, D. B. A., K. W. Bowman, P. I. Palmer, J. R. Worden, D. J. Jacob, R. N. Hoffman, I. Bey, and R. M. Yantosca (2003), Potential of observations from the Tropospheric Emission Spectrometer to constrain continental sources of carbon monoxide, *J. Geophys. Res.*, 108(D24), 4789, doi:10.1029/2003JD003702.
- Kuang, Z. M., G. C. Toon, P. O. Wennberg, and Y. L. Yung (2003), Measured HDO/H<sub>2</sub>O ratios across the tropical tropopause, *Geophys. Res. Lett.*, 30(7), 1372, doi:10.1029/2003GL017023.
- Lawrence, J. R., S. D. Gedzelman, X. P. Zhang, and R. Arnold (1998), Stable isotope ratios of rain and vapor in 1995 hurricanes, *J. Geophys. Res.*, 103(D10), 11,381–11,400.
- Lawrence, J. R., S. D. Gedzelman, D. Dexheimer, H. K. Cho, G. D. Carrie, R. Gasparini, C. R. Anderson, K. P. Bowman, and M. I. Biggerstaff (2004), Stable isotopic composition of water vapor in the tropics, *J. Geophys. Res.*, 109, D06115, doi:10.1029/2003JD004046.
- Moyer, E. J., R. W. Irion, Y. L. Yung, and M. R. Gunson (1996), ATMOS stratospheric deuterated water vapor and implications for tropospheric-stratospheric exchange, *Geophys. Res. Lett.*, 23, 2385–2388.
- Noone, D., and I. Simmonds (2002), Associations between d18O of water and climate parameters in a simulation of atmospheric circulation for 1979–1995, *J. Clim.*, 15(22), 3150–3169.
- Parker, R. L. (1994), *Geophysical Inverse Theory*, Princeton Univ. Press, Princeton, N. J.
- Rinsland, C. P., M. R. Gunson, J. C. Foster, R. A. Toth, C. B. Farmer, and Zander (1991), Stratospheric profiles of heavy water isotopes and CH<sub>3</sub>D in the analysis of ATMOS Spacelab 3 infrared spectra, *J. Geophys. Res.*, 96, 1057–1068.
- Rodgers, C. D. (2000), *Inverse Methods for Atmospheric Sounding: Theory and Practice*, World Sci., Tokyo.
- Rodgers, C. D., and B. J. Connor (2003), Intercomparison of remote sounding instruments, *J. Geophys. Res.*, 108(D3), 4116, doi:10.1029/2002JD002299.
- Rothman, L. S., et al. (2003), The HITRAN molecular spectroscopic database: Edition of 2000 includes updates through 2001, *J. Quant. Spectrosc. Radiat. Transfer*, 82(1–4), 5–44.
- Toth, R. A. (1999), HDO and D<sub>2</sub>O low pressure, long path spectra in the 600–3100 cm<sup>-1</sup> region I. HDO line positions and strengths, *J. Molec. Spectrosc.*, 195(1), 73–97.
- Webster, C. R., and A. J. Heymsfield (2003), Water isotope ratios D/H, O-18/O-16, O-17/O-16 in and out of clouds map dehydration pathways, *Science*, 302(5651), 1742–1745.
- Worden, J. R., K. W. Bowman, and D. B. Jones (2004a), Two-dimensional characterization of atmospheric profile retrievals from limb sounding observations, *J. Quant. Spectrosc. Radiat. Transfer*, 86(1), 45–71.
- Worden, J., S. S. Kulawik, M. W. Shephard, S. A. Clough, H. Worden, K. Bowman, and A. Goldman (2004b), Predicted errors of tropospheric emission spectrometer nadir retrievals from spectral window selection, *J. Geophys. Res.*, 109, D09308, doi:10.1029/2004JD004522.
- Zakharov, V. I., R. Imasu, K. G. Griбанov, G. Hoffmann, and J. Jouzel (2004), Latitudinal distribution of the deuterium to hydrogen ratio in the atmospheric water vapor retrieved from IMG/ADEOS data, *Geophys. Res. Lett.*, 31, L12104, doi:10.1029/2004GL019433.

---

R. Beer, K. Bowman, A. Eldering, B. Fisher, M. Gunson, R. Herman, S. S. Kulawik, M. Luo, G. Osterman, S. Sander, H. Worden, and J. Worden, Earth and Space Sciences Division, Jet Propulsion Laboratory, 4800 Oak Grove Drive, MS 183-301, Pasadena, CA 91109, USA. (john.worden@jpl.nasa.gov)

S. Clough and M. Shephard, Atmospheric and Environmental Research Inc. (AER), 131 Hartwell Avenue, Lexington, MA, 02421, USA.

A. Goldman, Department of Physics, University of Denver, 2112 E. Wesley Ave, Denver, CO 80208, USA.

M. Lampel, Raytheon Information Solutions, 299 N. Euclid Avenue, Suite 500, Pasadena, CA 91101, USA.

D. Noone, PAOS & CIRES, University of Colorado, Boulder, UCB 311, Boulder, CO 80309-0311, USA.

C. Rinsland, NASA Langley Research Center, Mail Stop 401A, Hampton, VA 23681-3142, USA.

C. Rodgers, Atmospheric, Oceanic and Planetary Physics, Clarendon Laboratory, Parks Road, Oxford OX1 3PU, UK.